The Astronomical Journal, 124:1776–1787, 2002 September

COMPARISON OF POSITIONS AND MAGNITUDES OF ASTEROIDS OBSERVED IN THE SLOAN DIGITAL SKY SURVEY WITH THOSE PREDICTED FOR KNOWN ASTEROIDS

Mario Jurić,[1,2] Željko Ivezić,[1] Robert H. Lupton,[1] Tom Quinn,[3] Serge Tabachnik,[1] Xiaohui Fan,[1]
James E. Gunn,[1] Gregory S. Hennessy,[4] Gillian R. Knapp,[1] Jeffrey A. Munn,[5]
Jeffrey R. Pier,[5] Constance M. Rockosi,[6] Donald P. Schneider,[7]
Jonathan Brinkmann,[8] István Csabai,[9] and Masataka Fukugita[10]
Received 2002 January 28; accepted 2002 May 16

ABSTRACT

We positionally correlate known asteroids with a sample of ~18,000 asteroids detected by the Sloan Digital Sky Survey (SDSS). We find 2641 unique matches, which represent the largest sample of asteroids with both accurate multicolor photometry and known orbital parameters. The matched objects are predominantly bright and demonstrate that the SDSS photometric pipeline recovers ~90% of the known asteroids in the observed region. For the recovered asteroids, we find a large offset (~0.4 mag) between Johnson V magnitudes derived from SDSS photometry and the predicted magnitudes. This offset varies with the asteroid color, from 0.34 mag for blue asteroids to 0.44 mag for red asteroids, and is probably caused by the use of unfiltered CCD observations in the majority of recent asteroid surveys. This systematic photometric error leads to an overestimate of the number of asteroids brighter than a given absolute magnitude limit by a factor of ~1.7. The distribution of the matched asteroids in orbital parameter space indicates strong color segregation. We confirm that some families are dominated by a single asteroid type (e.g., the Koronis family by red asteroids and the Themis family by blue asteroids), while others appear to be a mixture of blue and red objects (e.g., the Nysa-Polana family). Asteroids with the bluest i^*-z^* colors, which can be associated with the Vesta family, show particularly striking localization in orbital parameter space.

Key words: minor planets, asteroids — solar system: general

1. INTRODUCTION

The Sloan Digital Sky Survey (SDSS) is a digital photometric and spectroscopic survey that will cover 10,000 deg^2 of the celestial sphere in the north Galactic cap and produce a smaller (~225 deg^2) but much deeper survey in the southern Galactic hemisphere (York et al. 2000 and references therein). The survey sky coverage will result in photometric measurements for about 50 million stars and a similar number of galaxies. The flux densities of detected objects are measured almost simultaneously in five bands (u, g, r, i, and z; Fukugita et al. 1996) with effective wavelengths of 3551, 4686, 6166, 7480, and 8932 Å, 95% complete[11] for point sources to limiting magnitudes of 22.0, 22.2, 22.2, 21.3, and 20.5 in the north Galactic cap.[12] Astrometric positions are accurate to about 0.″1 per coordinate (rms) for sources brighter than 20.5 mag (Pier et al. 2002), and the morphological information from the images allows robust star-galaxy separation to ~21.5 mag (Lupton et al. 2002).

SDSS, although primarily designed for observations of extragalactic objects, will significantly contribute to studies of solar system objects because asteroids in the imaging survey must be explicitly detected to avoid contamination of the samples of extragalactic objects selected for spectroscopy. Ivezić et al. (2001, hereafter I01) analyzed SDSS commissioning data and showed that SDSS will increase the number of asteroids with accurate five-color photometry by more than 2 orders of magnitude (to about 100,000), and to a limit about 5 mag fainter (7 mag when the completeness limits are compared) than previous multicolor surveys (e.g., the Eight-Color Asteroid Survey, by Zellner, Tholen, & Tedesco 1985). The main results derived from these early SDSS observations are the following:

[1] Princeton University Observatory, Peyton Hall, Princeton, NJ 08544-1001.
[2] Department of Physics, University of Zagreb, Bijenička cesta 32, HR-10002 Zagreb, Croatia; and Višnjan Observatory, Istarska 5, HR-52463 Višnjan, Croatia.
[3] Department of Astronomy, University of Washington, Box 351580, Seattle, WA 98195.
[4] US Naval Observatory, 3450 Massachusetts Avenue, NW, Washington, DC 20392-5420.
[5] US Naval Observatory, Flagstaff Station, P.O. Box 1149, Flagstaff, AZ 86002.
[6] Department of Astronomy and Astrophysics, University of Chicago, 5640 South Ellis Avenue, Chicago, IL 60637.
[7] Department of Astronomy and Astrophysics, Pennsylvania State University, University Park, PA 16802.
[8] Apache Point Observatory, P.O. Box 59, Sunspot, NM 88349.
[9] Department of Physics and Astronomy, Johns Hopkins University, 3400 North Charles Street, Baltimore, MD 21218-2686; and Department of Physics of Complex Systems, Eötvös Loránd University, Pf. 32, H-1117 Budapest, Hungary.
[10] Institute for Cosmic Ray Research, University of Tokyo, 3-2-1 Midori, Tanashi, Tokyo 188-8502, Japan; and Institute for Advanced Study, Einstein Drive, Princeton, NJ 08540.

[11] These values are determined by comparing multiple scans of the same area obtained during the commissioning year. Typical seeing in these observations was 1.″5 ± 0.″1.

[12] We refer to the measured magnitudes in this paper as u^*, g^*, r^*, i^*, and z^* because the absolute calibration of the SDSS photometric system (dependent on a network of standard stars) is still uncertain at the ~0.03 mag level. The SDSS filters themselves are referred to as u, g, r, i, and z. All magnitudes are given on the AB_ν system (Oke & Gunn 1983; for additional discussion regarding the SDSS photometric system, see Fukugita et al. 1996 and Stoughton et al. 2002).

1. A measurement of the main-belt asteroid size distribution to a significantly smaller size limit (<1 km) than possible before. The size distribution resembles a broken power law, independent of the heliocentric distance: $D^{-2.3}$ for 0.4 km $\lesssim D \lesssim$ 5 km, and D^{-4} for 5 km $\lesssim D \lesssim$ 40 km.

2. A smaller number of asteroids compared with previous work. In particular, the number of asteroids with diameters larger than 1 km is about 7×10^5.

3. The distribution of main-belt asteroids in four-dimensional SDSS color space is strongly bimodal, and the two groups can be associated with S-type (rocky) and C-type (carbonaceous) asteroids, in agreement with previous studies based on smaller samples (Chapman, Morrison, & Zellner 1975; Zellner 1979). A strong bimodality is also seen in the heliocentric distribution of asteroids: the inner belt is dominated by S-type asteroids centered at $R \sim 2.8$ AU, while C-type asteroids, centered at $R \sim 3.2$ AU, dominate the outer belt.

It was demonstrated in I01 that the SDSS photometric pipeline ("Photo"; Lupton et al. 2002) is a robust and highly efficient automated tool for finding moving objects. I01 presents a detailed discussion of the completeness and reliability of the SDSS asteroid catalog based on the known SDSS photometric and astrometric precision, but this discussion is incomplete because it does not attempt a direct comparison with known asteroids on an object-by-object basis. The importance of such an analysis is evident from the realization that there are ~90,000 *known* asteroids with $H < 15.5$, while I01 expected to find only ~58,000 in the same absolute magnitude[13] range. The implied low completeness of 64% (compare with 98% estimated in I01) can only be verified by direct matching of known and SDSS asteroids.[14]

Another motivation for cross-correlating SDSS asteroids and known asteroids is a large potential increase in the number of asteroids with both accurate multicolor photometry and known orbital parameters (the SDSS data themselves are insufficient for accurate orbit determination but will provide serendipitous photometric measurements for a substantial fraction of known asteroids). In addition, the SDSS color information may be utilized to study the chemical segregation in the full orbital parameter space, rather than only as a function of heliocentric distance as done in I01.

This paper presents the first results on cross-correlating SDSS asteroids and known asteroids. Section 2 describes the analyzed data, a software pipeline used for generating the positions of known asteroids at the time of SDSS observations, and their positional matching to objects automatically detected by the SDSS photometric pipeline. Section 3 discusses the statistics of matched objects and compares the SDSS photometric measurements with the apparent magnitudes predicted from known absolute magnitudes. In § 4, we discuss the chemical segregation of asteroids in orbital element space, and in § 5 we summarize the main results.

2. MATCHING SDSS MOVING OBJECTS AND KNOWN ASTEROIDS

2.1. *SDSS Data*

We use asteroid data (cf. I01) from the SDSS Early Data Release (EDR), described in detail by Stoughton et al. (2002). These data include equatorial observing runs 94, 125, 752, and 756 (see I01 and Stoughton et al.); the boundaries are given by $-1.^\circ27 \lesssim$ decl. $\lesssim 1.^\circ27$ and R.A. = 351°–56° (runs 94 and 125) or R.A. = 145°–250° (runs 752 and 756). For a footprint in ecliptic coordinates, see Figure 1 in I01. This region has an area of 432 deg^2 and includes 12,668 moving objects selected as in I01 (velocity $v > 0.^\circ03$ day^{-1} and $14.0 < r^* < 21.5$). We use this sample for all quantitative estimates of the catalog completeness, and for photometric comparison. In order to increase the number of objects when studying the color segregation in the asteroid belt (§ 4), we also add additional objects from seven currently unreleased equatorial observing runs[15] that roughly double the matched sample size.

The SDSS photometric data include a list of objects flagged as moving by the photometric pipeline. For each object, the position and time of observation, and the magnitudes and associated errors in five SDSS photometric bands (*ugriz*), are recorded. The SDSS imaging data are obtained in the TDI (time-delay and integrate, or "drift scanning") mode,[16] and thus each observed position corresponds to a different observing time (as opposed to the staring mode, in which all objects from a given image are observed at the same time). In a general case, the correlation between a position and time is easiest to compute in the great-circle coordinate system. Since all the scans discussed here were obtained along the celestial equator, this dependence becomes particularly simple and is given by

$$T(\mathrm{RA}) = T_0 + \frac{\mathrm{RA} - \mathrm{RA}_0}{360^\circ} \text{ days}, \quad (1)$$

where T is the time corresponding to position RA (e.g., Julian day) and the zero points T_0 and RA_0 are constants for a given run (all reported positions correspond to the r band). For an arbitrary run, this expression is easily generalized by using an appropriate coordinate system.

The magnitudes for known asteroids are reported in the Johnson V band. Preliminary transformations from the SDSS photometric system to the Johnson bands are given by Fukugita et al. (1996) and Krisciunas, Margon, & Szkody (1998). We use a recently updated version of these transformations (M. Fukugita 2001, private communication; the new transformations produce V magnitudes that agree to better than 0.1 mag with the version from Fukugita et al. 1996) to synthesize the Johnson[17] B- and V-band magnitudes:

$$V_0 = r^* + 0.44(g^* - r^*) - 0.02, \quad (2)$$

$$(B - V)_0 = 1.04(g^* - r^*) + 0.19. \quad (3)$$

[13] The absolute magnitude is the magnitude that an asteroid would have at a distance of 1 AU from the Sun and from Earth, viewed at zero phase angle. For more details, see I01 and references therein.

[14] We thank R. Jedicke for pointing out this discrepancy to us.

[15] Prompt release of asteroid data (i.e., without any waiting period) is currently under consideration by SDSS.

[16] See http://www.astro.princeton.edu/PBOOK/welcome.htm.

[17] Although SDSS has already produced more multicolor photometric measurements of asteroids than are available in the Johnson system, we use the Johnson system to ease comparison with earlier studies.

For typical values of g^*-r^* for asteroids (0.4–0.8), V_0-r^* is in the range 0.16–0.33. The overall accuracy of these transformations and SDSS photometry is better than $\sim$0.05 mag, as determined by direct comparison with non-SDSS observations obtained in the Johnson system (M. Fukugita, E. Grebel, & J. Holtzman, unpublished).

2.2. *The Asteroid Orbital Elements Database*

For positional matching of the moving objects observed by SDSS with known asteroids, we select the Asteroid Orbital Elements Database (ASTORB). ASTORB is a file with high-precision osculating orbital elements and other information on all numbered and a large number of unnumbered asteroids (but does not contain information on known numbered comets). ASTORB is distributed by Lowell Observatory in the form of an ASCII file, containing single-line records for each asteroid.[18] The ASTORB file is updated daily for addition of newly discovered objects, deletion of duplicate objects, and improvement of parameters of known objects. In this work, we use the six osculating orbital elements, absolute magnitude, and the phase correction slope parameter, which are necessary to predict the asteroid position and apparent magnitude at the time of SDSS scans. We also utilize the arc (in days) spanned by the observations used to compute the orbit, to estimate the accuracy of the orbital elements.

Orbital elements given in ASTORB are heliocentric and have been computed by a variable time step differential orbit correction algorithm, based on astrometric observations obtained from the Minor Planet Center (MPC). The perturbations from all the major planets, the Moon, and the three largest asteroids (Ceres, Pallas, and Vesta) have been taken into account. Absolute magnitude corresponding to the Johnson V band (H; see I01) is listed as numbers rounded to two, one, or no decimal places, with the number of decimal places reflecting assumed reliability. However, for unnumbered asteroids H is given to two decimal places regardless of its real accuracy. The slope parameter G (see § 2.3.2 below) is given for asteroids for which it is known and, for others, which are the overwhelming majority of the sample, assumed to be 0.15 (dimensionless).

We note that besides ASTORB there are several other asteroid orbital elements databases (e.g., the Minor Planet Center Orbit Database[19] and the Asteroid Dynamics Site[20]). However, because of its widespread use and significant additional information supplied for each asteroid, we have chosen to use ASTORB as a reference for this study. The ASTORB version used here is from 2001 September 18 and contains 141,110 objects (29,074 of which are numbered asteroids).

2.3. *Asteroid Identification Pipeline*

The asteroid identification pipeline consists of three parts:

1. Propagation of the asteroid osculating orbital elements from ASTORB to the epoch of the SDSS observation;
2. Computation of the asteroid positions and apparent magnitudes at the time of SDSS scan; and
3. Positional matching of SDSS moving objects with the known asteroids.

2.3.1. *Propagation of Orbits*

The ASTORB file contains osculating orbital elements computed for epochs near the current epoch, where "current" corresponds to the publication date of the ASTORB file. The orbital elements are propagated to the epoch of observation using the PROELE routine of the OrbFit version 1.8 PROPAG library (Milani 1999). We use the default dynamical model supplied with the OrbFit package. It includes gravitational perturbations from the Sun, Moon, and the major planets and relativistic corrections, when necessary. The positions and masses for major planets are derived from JPL ephemeris DE405 (Standish 1998). Although the OrbFit package offers multiple choices for the numerical integration scheme, we use its automated selection procedures, which have proved to be sufficiently accurate in practice (Jurić & Korlević 2000). The end result of the orbit propagation is a list of osculating orbital elements at the time of SDSS observation, which are then used for quick two-body (Sun and asteroid) computations of the ephemeris.

2.3.2. *Computation of Asteroid Positions and Apparent Magnitudes*

The calculations of positions are performed using a modified PREOBS routine from the same OrbFit package (the modification consists of enabling a two-body approximation). When calculating the positions of known asteroids, they must satisfy the condition given by equation (1). We solve the problem iteratively, until the difference between the positions calculated in two successive iterations is smaller than $0''.001$. In practice, the computations converge rapidly and usually reach the required accuracy with two to three iterations.

The apparent magnitudes are computed by OrbFit's APPMAG subroutine from the values of the absolute magnitude H and the phase correction slope parameter G listed in the ASTORB file. The phase-corrected apparent visual "catalog" magnitude V_c is obtained from

$$V_c(\alpha) = H + 5\log(R\Delta) - 2.5\log[(1-G)\Phi_1(\alpha) + G\Phi_2(\alpha)] \quad (4)$$

(Bowell et al. 1989), where R is the heliocentric, and Δ is the geocentric, distance (expressed in AU), α is the "solar" angle (the angle between the Sun and Earth as viewed from the asteroid; see I01), and Φ_1 and Φ_2 are the "phase correction" functions. The latter are obtained from standard approximations:

$$\Phi_i = \exp[-A_i(\tan\tfrac{1}{2}\alpha)^{B_i}], \quad i = 1,2\ ; \quad (5)$$

$$A_1 = 3.33\ , \quad A_2 = 1.87\ , \quad B_1 = 0.63\ , \quad B_2 = 1.22\ . \quad (6)$$

Note that these approximations are formally different from that used by I01 (their eq. [11]). However, they are similar numerically; the difference is less than 0.05 mag for $\alpha < 2^\circ$ and $\alpha \sim 6^\circ$, with the maximum value of $\sim$0.15 mag at $\alpha \sim 3^\circ$.

2.4. *Matching Algorithm*

The matching algorithm compares the list of predicted positions for the known asteroids with the list of SDSS

[18] See ftp://ftp.lowell.edu/pub/elgb/astorb.html.
[19] Available from ftp://cfa-ftp.harvard.edu/pub/MPCORB.
[20] Available from http://hamilton.dm.unipi.it/cgi-bin/astdys/astibo.

objects flagged as moving by the photometric pipeline. After finding the nearest neighbor pairs from the two lists, it requires that the distance between the two positions be less than 30″. The final sample is very insensitive to the precise value of this cut, because for the majority (86%) of matched objects the distance between the two positions is less than 3″ (centered on zero in both coordinates). The probability that a randomly chosen position would fall within 3″ from a moving SDSS object is of order 10^{-4} in the regions with the highest asteroid number density (64 deg^{-2}; I01), implying that only about one of the matches within 3″ is a random association. The associated objects are taken to be positive positional identifications of an SDSS moving object with a known asteroid.

3. THE MATCHING RESULTS

The SDSS photometric pipeline identified 12,668 moving objects selected as described in I01. There are 2801 known asteroids whose computed positions are within the boundaries of the SDSS scans considered here, and 1633 have within 30″ an object flagged by the SDSS photometric pipeline as moving. Of these, only 1325 are unique objects, because some asteroids were observed by SDSS more than once (I01). Detailed statistics for each run are listed in Table 1.

This comparison, taken at face value, implies that the SDSS sample is 58% complete. This is a much lower completeness than claimed in I01 (98%). We have visually inspected SDSS images around the positions of all 1168 ASTORB objects not found in the SDSS catalog (moving objects are easily recognized on 1′ × 1′ *gri* color composites thanks to their peculiar appearances; see I01). There are 219 objects that are clearly moving but were not recognized as such by the photometric pipeline. The most common reason for missing them is complex environments (bright stars with diffraction spikes, compact galaxy clusters, meteor and airplane trails, etc.), which are hard to "deblend" into individual sources. The revised, true completeness of the SDSS sample is thus 88%, somewhat lower than the 98% determined in I01. We note that I01 determined completeness using only data from run 756. For this run, the completeness determined here is 91%. Furthermore, for all runs except run 94 the completeness is higher than 90%. The overall completeness is below 90% only for run 94 (81%), which is one of the earliest SDSS commissioning runs, obtained while the telescope still did not have proper optics.

For the remaining 949 (34% of the total) ASTORB objects, there is no visible SDSS source within 30″ of the predicted position down to the sensitivity limit of $r^* \sim 22.5$. The most plausible explanation for these "missing" sources is inaccurate orbital elements (that is, their true position during SDSS observations is farther than 30″ from the predicted position). Indeed, the inspection of their entries in the ASTORB file indicates that the majority either are faint ($H \gtrsim 17$), have a small observational arc used to determine the orbital elements, or both.

3.1. *Selection of Asteroids with Reliable Orbital Elements*

SDSS observations demonstrate that a large fraction of known asteroids listed in the ASTORB file do not have sufficiently accurate orbital elements for reliable identification. The observational arc used to determine the orbital elements can be utilized as a rough estimate of their quality—the longer the arc spanned by the observations used to compute the elements, the more accurate the positions. The ASTORB file also provides a more quantitative estimate for the accuracy of the orbital elements—the *current ephemeris uncertainty* (CEU) parameter (1 σ absolute positional uncertainty), for an epoch near its publication date. However, the CEU cannot be propagated to the time of observation without knowledge of the covariance matrices for the orbital elements solution (cf. Muinonen & Bowell 1993), and we use arc to make a quality cut.

The relationship between the CEU and the arc is shown in Figure 1. The top panel shows each object from the ASTORB file as a dot, and the bottom panel shows the arc histogram for all objects by a solid line, and separately for objects with CEU > 30″ as the hatched region. As is evident, the requirement that the arc be greater than 300 days successfully eliminates most of the asteroids with large CEUs and selects 1634 objects (out of 2801). Note that the resulting sample is insensitive to the precise value of this cutoff because of the noncontinuous distribution of data. A further constraint is based on the predicted apparent magnitude. We only select asteroids that are reliably detectable by SDSS; they satisfy $14 \leq V_c \lesssim 21.5$ (I01). This cut has only minor importance and selects 1612 objects (relaxing the limit to 22.5 adds three objects).

The absolute magnitudes for selected (hereafter "reliable") and removed (hereafter "unreliable") asteroids are compared in Figure 2. The solid line shows the absolute magnitude distribution for all 2801 asteroids, and the dashed and dotted lines show the distributions for the 1612 (58%) reliable and 1189 (42%) unreliable asteroids, respectively. It is evident that the asteroids with unreliable orbital parameters are mostly faint, and they dominate the sample for $H > 15.5$. The subsample of reliable asteroids appears complete for $H < 14$.

The removal of the sources with unreliable orbital elements is efficient, but not perfect. The matching statistics for

TABLE 1

ALL ASTORB ASTEROIDS MATCHED TO SDSS OBJECTS

Run	ASTORB Asteroids	SDSS Objects	Matched Objects	Missed by Photo	Not Found ASTORB
94	663	2757	395	94	174
125	648	2844	426	48	174
752	712	3422	373	33	306
756	778	3645	439	44	295
All	2801	12668	1633	219	949
Unique	2170		1325		

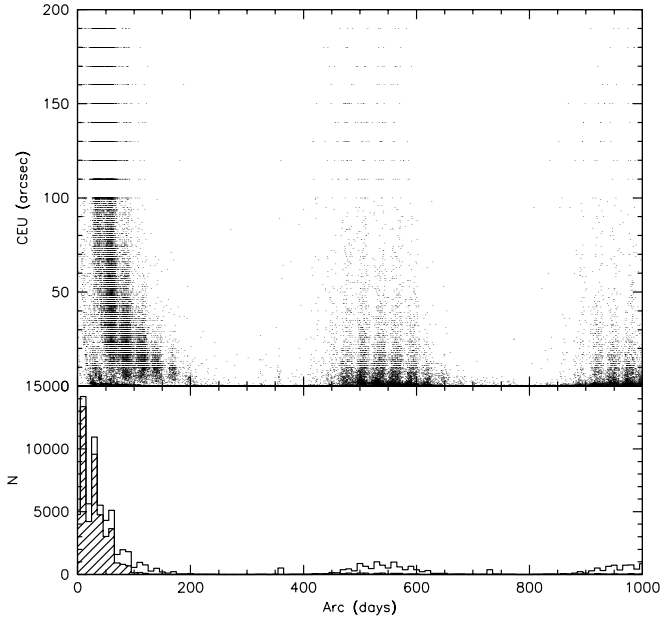

FIG. 1.—*Top*: Relation between the observational arc and the current ephemeris uncertainty for the 141,110 objects from the ASTORB file (*dots*). The discretization is caused by truncation. *Bottom*: Arc histograms for all objects and, separately, for objects with CEU $> 30''$ (*hatched area*). As is evident, most of the latter are concentrated in the first peak and are eliminated by the condition that the arc be greater than 300 days.

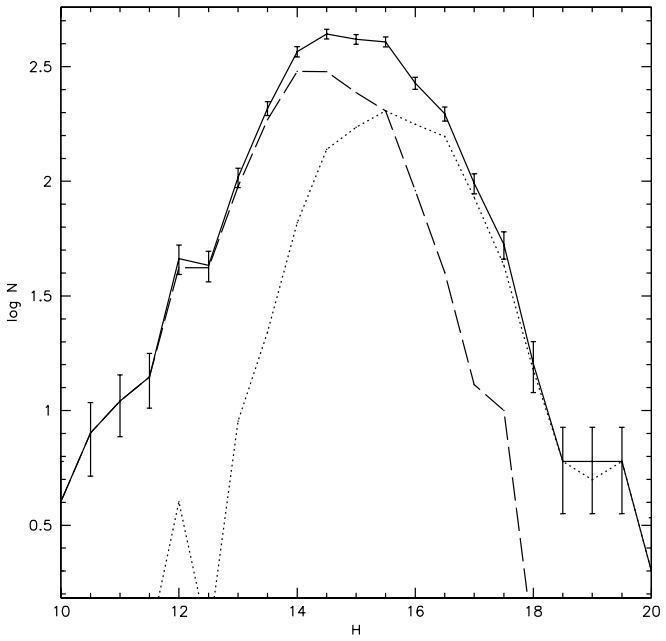

FIG. 2.—*Solid line*, absolute magnitude distribution for the 2801 known asteroids from the ASTORB database that are expected to be observed in the SDSS scans discussed here; *dashed line*, distribution for the 1612 asteroids with the most reliable orbital elements; *dotted line*, distribution for the remaining sources, with less reliable orbital elements.

the subsample of ASTORB asteroids with reliable orbits is listed in Table 2. Out of 1612 objects, 1335 are matched within $30''$ to objects automatically recognized by the photometric pipeline as moving. Of the remaining 277 objects, 173 are visually identified as moving, and the remaining 104 objects do not have an SDSS moving source within $30''$. For each of these 104 objects, the predicted position has been independently verified using the on-line AstDyS orbital calculator.[21] In summary, the arc > 300 days cut decreases the fraction of ASTORB asteroids with unreliable orbital elements from 34% to 6%. The SDSS completeness based on the reduced sample is 89% (=1335/1508), consistent with the estimate based on the full sample (88%). Since the removed objects are predominantly faint, this agreement indicates that the SDSS completeness is not strongly dependent on apparent magnitude.

[21] Available from http://hamilton.dm.unipi.it/cgi-bin/astdys/astibo.

3.2. *The Matching Statistics*

The sample of 1335 matched objects that were detected by the photometric pipeline, together with the sample of 173 visually confirmed objects from the ASTORB file, can be used to determine whether the completeness of the SDSS automatically detected sample depends on magnitude. The top panel in Figure 3 compares the absolute magnitude distribution, as listed in the ASTORB file, for the 1335 matched objects (*dashed line*) with the distribution of all 1508 objects (*solid line*). The bottom panel shows the fraction of matched sources in each magnitude bin (*dotted line with error bars*). The horizontal line is added to guide the eye and represents the overall completeness of 89%. As is evident, there is no significant correlation between the fraction of matched sources and the magnitude.

We have also tested for correlations between the fraction of matched sources and the phase angle, the object's color, and apparent magnitude and did not find any significant dependences.

TABLE 2
RELIABLE ASTORB ASTEROIDS MATCHED TO SDSS OBJECTS

Run	ASTORB Asteroids	SDSS Objects	Matched Objects	Missed by Photo	Not Found ASTORB
94	391	2757	290	82	19
125	402	2844	350	32	20
752	374	3422	318	25	31
756	445	3645	377	34	34
All	1612	12668	1335	173	104
Unique	1239		960		

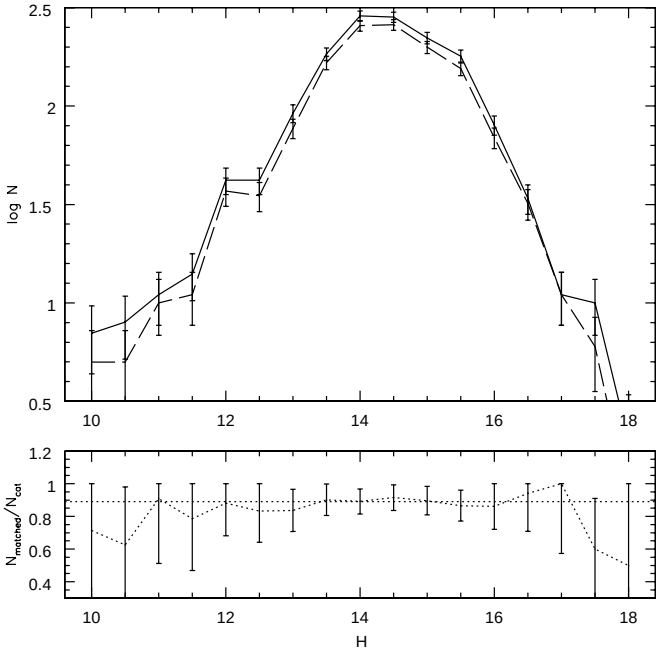

FIG. 3.—*Top*: Absolute magnitude distribution, as listed in the ASTORB file, for the 1335 objects recognized as moving by the SDSS photometric pipeline and matched within 30″ to an object from the ASTORB file (*dashed line*), and the distribution of all 1508 moving objects selected from the ASTORB file (*solid line*). *Bottom*: Fraction of matched sources in each magnitude bin, shown by the dotted line with error bars. The horizontal line is added to guide the eye and represents the overall SDSS completeness of 89%. Note that there is no significant correlation between the fraction of matched sources and the magnitude.

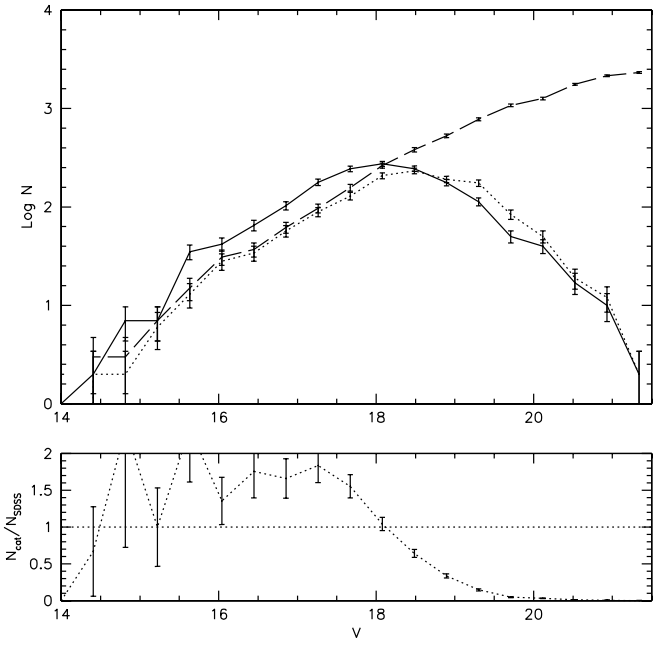

FIG. 4.—*Top*: Comparison of the apparent magnitude distribution for asteroids from the ASTORB file that are within the boundaries of SDSS scans discussed here (*solid line*) with the apparent magnitude distributions for moving objects detected by SDSS. The distribution for all SDSS objects is shown by the dashed line, and the distribution for matched objects by the dotted line. *Bottom*: Number ratio of ASTORB and SDSS asteroids in each magnitude bin. Although it appears that the SDSS completeness is as low as 60% for $V \sim 17.5$, the SDSS catalog includes 89% of ASTORB asteroids, and the mismatch is due to an offset in the apparent magnitude scales.

3.2.1. *Apparent Magnitude Distribution*

The top panel in Figure 4 compares the apparent magnitude distribution for asteroids from the ASTORB file that are within the boundaries of the SDSS scans discussed here (*solid line*) with the apparent magnitude distributions for moving objects detected by SDSS. The distribution for all SDSS objects is shown by the dashed line, and the distribution for matched objects by the dotted line. We use the calculated V_c magnitudes for the ASTORB asteroids and synthesized V_0 magnitudes for SDSS asteroids (including the matched sample; this is why the dotted line is above the solid line for $V \gtrsim 19$). At first sight, it appears that the SDSS sample is significantly incomplete. The bottom panel shows the number ratio of ASTORB and SDSS asteroids in each magnitude bin and indicates that the SDSS completeness is as low as 60% for $V \sim 17.5$. However, as demonstrated in the previous section (see Fig. 3), the SDSS catalog *includes* 89% of ASTORB asteroids, and the mismatch in Figure 4 is simply due to an offset in apparent magnitude scales.

The existence of such an offset is further corroborated by a direct comparison of the calculated (V_c, based on the ASTORB file) and synthesized (V_0, based on SDSS observations) magnitudes for the 1335 matched objects. The top panel in Figure 5 shows the histogram of the difference $V_0 - V_c$ for all 1335 objects by the solid line. The median offset is 0.41 mag (the SDSS values are fainter), with rms of 0.35 mag. The dotted and dashed lines show $V_0 - V_c$ histograms for the 400 blue asteroids and the 935 red asteroids selected by their a^* color, as described in I01. It is evident that the apparent magnitude offset depends on the asteroid

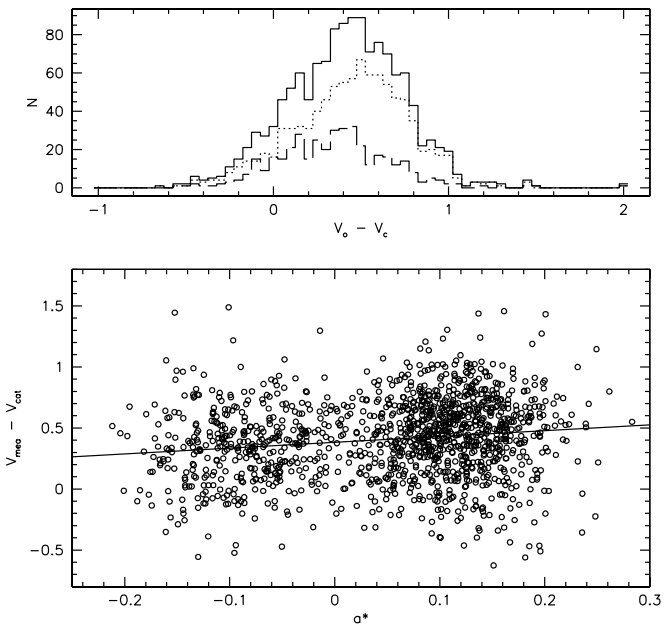

FIG. 5.—*Top*: The $V_0 - V_c$ histogram for all 1335 objects (*solid line*). The dotted and dashed lines show the analogous histograms for the 400 blue asteroids and the 935 red asteroids, respectively. *Bottom*: The $V_0 - V_c$ difference as a function of the asteroid color a^*, and a best linear fit.

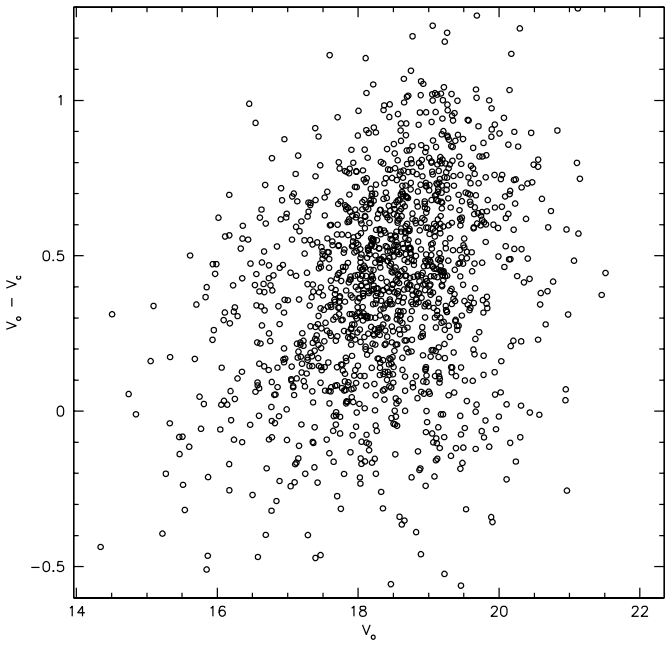

FIG. 6.—The $V_0 - V_c$ difference for all 1335 objects as a function of V_0.

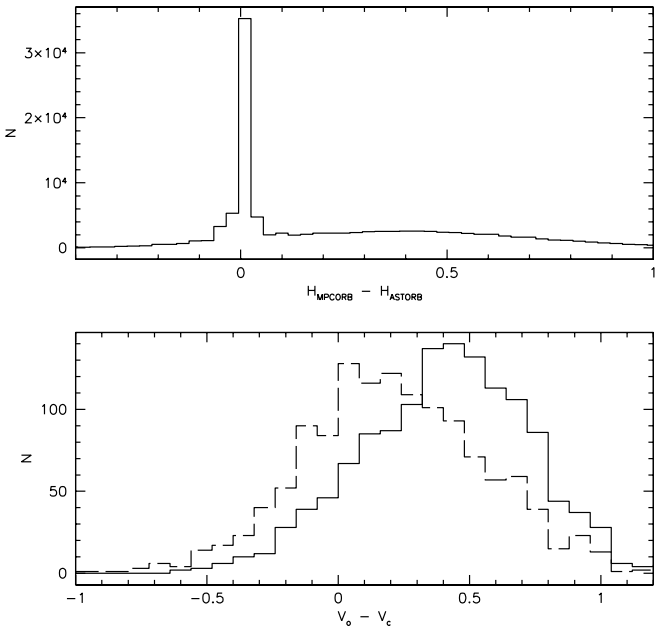

FIG. 7.—*Top*, comparison of the difference in absolute magnitudes for the 115,583 common objects listed in the MPC and ASTORB files; *bottom*, comparison of the difference between the magnitude observed by SDSS and predicted magnitudes for the ASTORB file (*solid line*) and for the MPC catalog (*dashed line*).

color; the median offsets are 0.34 and 0.44 for the blue and red subsamples, respectively. This dependence is further illustrated in the bottom panel, where the $V_0 - V_c$ difference is plotted as a function of the asteroid color a^*. The $V_0 - V_c$ histograms shown in Figure 5 are not symmetric and give a hint of two components: one centered at ~0.1 that is independent of color, and another centered at ~0.4–0.5 that appears to be color dependent. This bimodality is more pronounced for $V \gtrsim 17$, as is discernible in Figure 6.

It is of obvious interest to find out whether the offset between predicted and observed magnitudes is particular to the ASTORB file or, perhaps, also present in other available databases. For this test, we chose the Minor Planet Center Orbit Database from 2001 September 5. It contains similar data to the ASTORB file for 115,797 objects; 115,583 of these objects are common to both catalogs. The top panel in Figure 7 compares the listed absolute magnitudes for the objects in common. As is evident, the catalogs contain two "populations" of objects. For about half of the sample the difference between the two values is less than 0.1 mag, while for the remaining 57,719 objects it is larger than 0.1. The median value for the latter is ~0.4. We did not find any correlation between the difference in absolute magnitude and other cataloged quantities. In particular, there is no correlation between this difference and the mean absolute magnitude. Given only two catalogs, it is not possible to tell which one is responsible for the offset in magnitude scale. Fortunately, the catalogs can be compared with SDSS observations of the matched objects for which the photometric errors are not larger than 0.05 mag. The bottom panel in Figure 7 compares the $V_0 - V_c$ histograms obtained with the data from the ASTORB file (*solid line*) and from the MPC file (*dashed line*). As is evident, the median discrepancy between the listed magnitudes and the magnitudes measured by SDSS is about twice as large for the ASTORB file as for the MPC file (~0.4 mag vs. ~0.2 mag). Based on this finding alone, it would seem that the MPC file should be used for the matching purposes. However, the MPC file contains fewer objects than does ASTORB; out of the 1633 matched objects, only 1387 are found in the MPC file (implying an upper limit on the completeness of the MPC file of 85%).

The discrepancy in the absolute magnitude scale significantly affects the number of objects brighter than a given limit. Assuming that the number counts follow a $\log N = C + 0.6V$ relation (I01), the MPC file will imply 1.32 more objects than SDSS measurements, and ASTORB will imply 1.74 more objects than SDSS measurements.

Although the uncertainty in the values of V_0 synthesized from the SDSS photometry is probably smaller than 0.05 mag, it is prudent to verify the offset in magnitude scales using non-SDSS observations. Krisciunas et al. (1998) obtained photometric measurements in SDSS-like bands for 15 bright asteroids. Table 3 lists their measurements and the synthesized, V_0, and predicted, V_c, magnitudes. The $V_0 - V_c$ difference is shown as a function of V_0 in Figure 8. Asteroids with H in the ASTORB file given to two decimal places are shown as circles, and those with one decimal place as triangles. The former are predominantly at the bright end, where they scatter around zero offset, indicating that the photometric transformations from SDSS to Johnson V band are not biased. The latter are found at the faint end and indicate a similar offset in the magnitude scales, as discussed above.

The correlation between the magnitude offset and the asteroid color indicates that the discrepancy is probably due to differences in the standard Johnson V magnitude and the "visual" magnitude listed in the ASTORB file. A most likely cause is the fact that the majority of current asteroid surveys (which produce most of the entries in the catalogs)

TABLE 3
PHOTOMETRIC OBSERVATIONS OF ASTEROIDS

Name	Type	Date (1997)	UT	r^*	g^*-r^*	V_{mea}[a]	V_{cat}[b]	$V_{mea}-V_{cat}$
446 Aeternitas	A	Sep 30	1109	14.33	0.61	14.58	13.43	1.14
702 Alauda	C	Sep 30	1147	12.75	0.45	12.93	12.90	0.03
82 Alkmene	S	Sep 28	1057	12.43	0.64	12.69	12.72	−0.02
774 Armor	S	Sep 28	0352	12.97	0.71	13.26	12.94	0.32
371 Bohemia	AS	Oct 4	0505	12.64	0.65	12.90	12.83	0.07
349 Dembowska	R	Sep 29	1154	10.28	0.70	10.57	10.57	0.00
433 Eros[a]	S	Sep 30	1226	13.30	0.67	13.57	13.09	0.48
480 Hansa	S	Sep 29	0959	12.25	0.63	12.51	12.61	−0.10
10 Hygiea	C	Sep 28	1205	11.43	0.46	11.61	11.54	0.06
683 Lanzia	C	Oct 1	0335	14.23	0.48	14.42	13.78	0.64
68 Leto	S	Sep 27	1037	10.11	0.66	10.38	10.53	−0.15
149 Medusa	S	Sep 29	0612	12.57	0.68	12.85	12.96	−0.11
196 Philomela	S	Sep 28	0851	11.41	0.64	11.67	11.56	0.10
314 Rosalia	C	Oct 5	0315	13.95	0.46	14.13	13.81	0.32
138 Tolosa	S	Oct 5	0411	11.57	0.69	11.85	11.92	−0.07

NOTE.—Observations with SDSS-like filters by Krisciunas et al. 1998.
[a] Synthesized Johnson V magnitude based on observations using SDSS-like filters.
[b] Predicted catalog-based Johnson V magnitude.

are obtained with open, unfiltered CCDs, since they are mostly concentrated on astrometric measurements. In addition, photometric observations are sometimes reported in the B and R bands, and the transformation to the V band is performed by applying a constant "correction" term. Since the asteroid colors have a finite range, this procedure must result in color-dependent photometric errors. Thus, the measured magnitudes are not equivalent to the standard Johnson V band, and furthermore, the discrepancy depends on the asteroid color.[22]

Indeed, as discussed by Jedicke, Larsen, & Spahr (2002), the reporting of observed asteroid magnitudes is notoriously inconsistent. For example, the MPC regularly weights magnitudes reported by different groups according to their historical photometric accuracy and transforms them to the V band, while ASTORB uses the unweighted photometry in observed bands in determining the absolute magnitude.

Correcting the predicted magnitudes for a median offset of 0.41 mag shifts the V_c histogram for ASTORB asteroids shown in Figure 4 by the right amount to make the matched fraction consistent with the estimate shown in Figure 3. We show the shifted histogram in Figure 9.

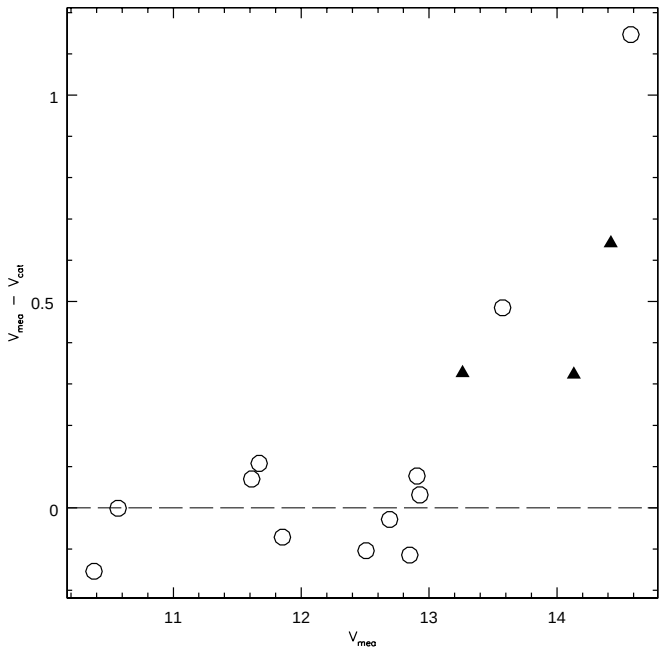

FIG. 8.—Differences between observed and calculated apparent V-band magnitudes of 15 asteroids observed by Krisciunas et al. (1998). Asteroids having absolute magnitudes accurately determined (given to two decimal places in the ASTORB catalog) are marked by circles. Triangles represent asteroids with poorly known absolute magnitudes (given to one decimal place). The dashed horizontal line serves as a visual aid, marking the position of zero magnitude difference.

4. COLOR SEGREGATION IN THE ASTEROID BELT

As discussed in § 2.1, we joined the 1335 matched objects from the SDSS Early Data Release with 1306 matched objects from unreleased runs, to form the final sample of 2641 unique matched objects. This is the sample used in our analysis of the color segregation in the asteroid belt.

4.1. *Asteroid Dynamical Families*

Asteroid dynamical families are groupings of asteroids in proper[23] orbital elements space, widely thought to be the results of collisional disruptions of parent bodies (larger asteroids). Pioneered by Hirayama (1918), our understand-

[22] The referee has pointed out that the correlation between the magnitude offset (0.1 mag) and the asteroid color could be partially due to the dependence of the slope parameter G (see § 2.3.2) on color. Assuming $G = 0.1$ for blue asteroids and $G = 0.25$ for red asteroids, we find that the expected difference in magnitudes due to adopting the same value of G is 0.02 ± 0.01.

[23] Proper orbital elements are nearly invariants of motion and thus are well suited for discovering objects with a common dynamical history. They are different from the osculating orbital elements, which describe the current motion. For more details, see Milani & Knežević (1992 and references therein).

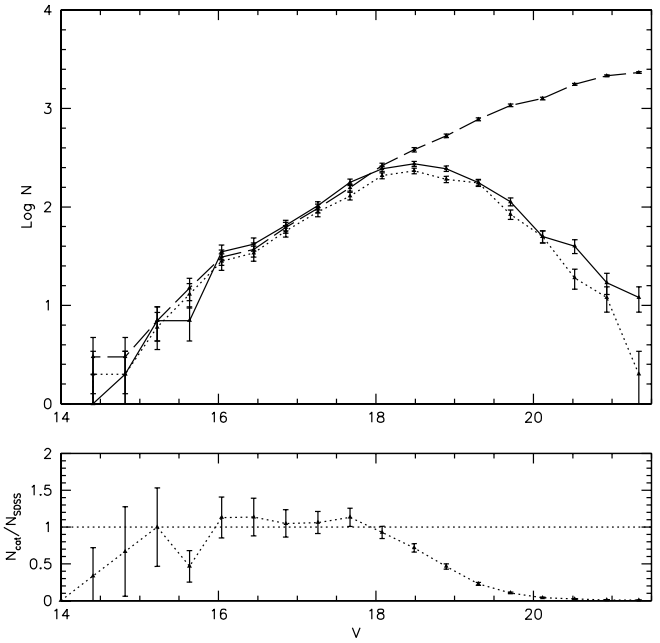

FIG. 9.—Apparent magnitude distributions as in Fig. 4, except that the predicted magnitudes for ASTORB asteroids were offset by 0.41 mag (*solid line*). The shifted distribution implies SDSS completeness in agreement with that shown in Fig. 3.

ing of asteroid families and the number of them known have increased dramatically thanks to a number of factors—a large increase in the number of discovered asteroids, more advanced knowledge of celestial mechanics, and more sophisticated cluster discovery techniques. For a detailed review, see Chapman et al. (1989).

In a recent study, Zappalà et al. (1995) identified 32 families and 31 "clumps" using a hierarchical clustering method in a sample of 12,487 asteroids. However, even a rough taxonomic classification exists for only a small number of these objects. Knowledge of the chemical composition of each family could provide further clues about the physical properties of the parent body. SDSS photometric data can remedy this problem, because the asteroids segregate in SDSS multidimensional color space. In this section, we analyze the correlation between SDSS colors and the distribution in orbital parameter space for 2641 matched asteroids.

In order to study the correlation between SDSS colors and the various taxonomic systems, we have cross-referenced the 1335 matched asteroids from the SDSS EDR sample with a catalog of asteroids with known taxonomy obtained at the Planetary Data System's Small Bodies Node. The catalog contains information on 1199 objects, with Tholen (978 objects), Barucci (438 objects), Tedesco (357 objects), Howell (112 objects), and Xu (221 objects) taxonomies. There are only seven asteroids with taxonomic information present in the SDSS sample, and these are listed in Table 4. This small number is not surprising given that the SDSS saturation limit ($V \sim 14$) is usually below the faint limit for most taxonomy surveys. The seven asteroids have SDSS colors in agreement with their taxonomic types (I01).

TABLE 4

ASTEROIDS WITH KNOWN TAXONOMY IN THE SDSS EDR SAMPLE

Asteroid	Taxonomy[a]	a^*	i^*-z^*
220 Stephania.....	XC (Tholen)	−0.062	−0.012
1628 Strobel.....	X (SMASS)	0.024	0.079
1679 Nevanlinna	X (SMASS)	−0.048	0.036
1711 Sandrine	S (Tholen)	0.074	0.042
1772 Gagarin	S (SMASS)	0.135	0.003
2215 Sichuan.....	S (SMASS)	0.097	0.011
5118 Elnapoul.....	S (SMASS)	0.151	−0.022

[a] Asteroid taxonomic classification and its source.

4.2. *Color Properties of Asteroid Families*

The 2641 known asteroids observed by SDSS have been cross-referenced with the catalog of proper orbital elements produced by Milani (1999) and distributed through AstDyS. The resulting sample includes 1768 asteroids with available proper elements. Hereafter we separate this sample into 531 blue asteroids ($a^* < 0$; see I01) and 1237 red asteroids ($a^* > 0$). As discussed in I01, there is a possibility that red asteroids with $i^*-z^* < -0.25$ form a separate group in color-color space, and we treat separately the 131 asteroids with such colors. In the remainder of this section, we analyze the differences in the distributions of these subsamples in the three-dimensional space spanned by the semimajor axis a', inclination i', and eccentricity e'.

Figure 10 displays the distribution of asteroids in the a' versus $\sin i'$ plane. The top panel shows 67,917 asteroids from the ASTORB database that have known proper orbital elements (from Milani 1999; *dots*). The major dynamical families (also known as the Hirayama families), Eos, Koronis, and Themis, are clearly visible at $a' > 2.8$ AU; their approximate $(a', \sin i')$-positions are (3.0, 0.18), (2.9, 0.03), and (3.15, 0.02), respectively. The 4 : 1, 3 : 1, 5 : 2, and 2 : 1 mean motion resonances with Jupiter at 2.065, 2.501, 2.825, and 3.278 AU (the latter three correspond to the Kirkwood gaps) are also evident. The ν_6 resonance is visible as a strong cutoff of asteroid density at high inclinations in the $2.065 < a' < 2.501$ region. Because we are using a sample that is about 5 times larger, the various families are more easily discerned than in Zappalà et al. (1995); however, the distribution shown here agrees with their results. The remaining two panels show the same distribution as isodensity contours, with the matched asteroids shown by circles. The middle panel shows blue asteroids ($a^* < 0$), and the bottom panel shows red asteroids ($a^* > 0$). A subset of red asteroids with $i^*-z^* < -0.25$ is shown by crosses; most are found around $a' \sim 2.2$–2.5 and $\sin i' \sim 0.12$. Figures 11 and 12 are analogous to Figure 10 and show the asteroid distributions in the e' versus a' and e' versus $\sin i'$ planes. Figure 12 shows the distributions in three belt regions selected by the positions of resonances.

For studying the chemical composition of various families, we adopt the family definitions of Zappalà et al. (1995). The distribution of blue and red asteroids in the a'-$\sin(i')$-e' space confirms the earlier results for the three largest families. The Koronis and Eos families seem to be mostly composed of red asteroids: 40 out of 45 (89%) asteroids associated with the Koronis family are red, and 77 of 98 (79%) are red for the Eos family. On the other hand, the Themis family is predominantly blue: 41 out of 43 (95%) members have $a^* < 0$. All three major families are located in the outer belt. From other families in the outer belt, we find two members of the Brasilia family; both are blue.

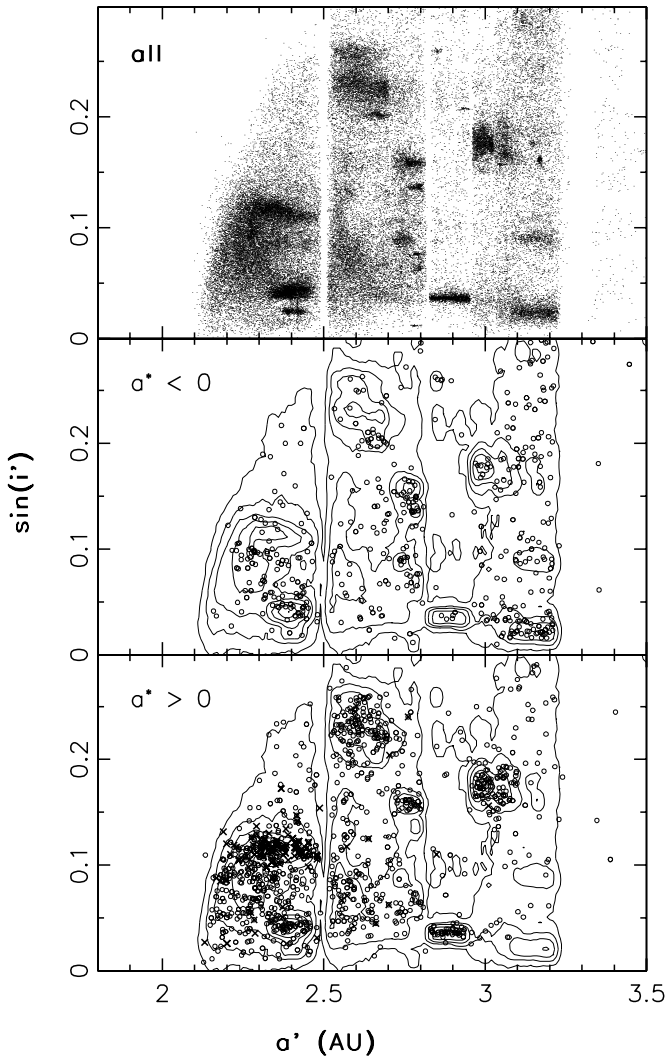

FIG. 10.—Distribution of asteroids in the sin i' vs. a' plane. The top panel shows 67,917 asteroids with the known proper orbital elements, marked as dots. The remaining two panels show the same distribution as isodensity contours, with the matched asteroids shows by open circles. The middle panel shows blue asteroids ($a^* < 0$), and the bottom panel shows red asteroids ($a^* > 0$). A subset of red asteroids with $i^* - z^* < -0.25$ is shown by crosses; most are found around $a' \sim 2.2$–2.5 and sin $i' \sim 0.12$.

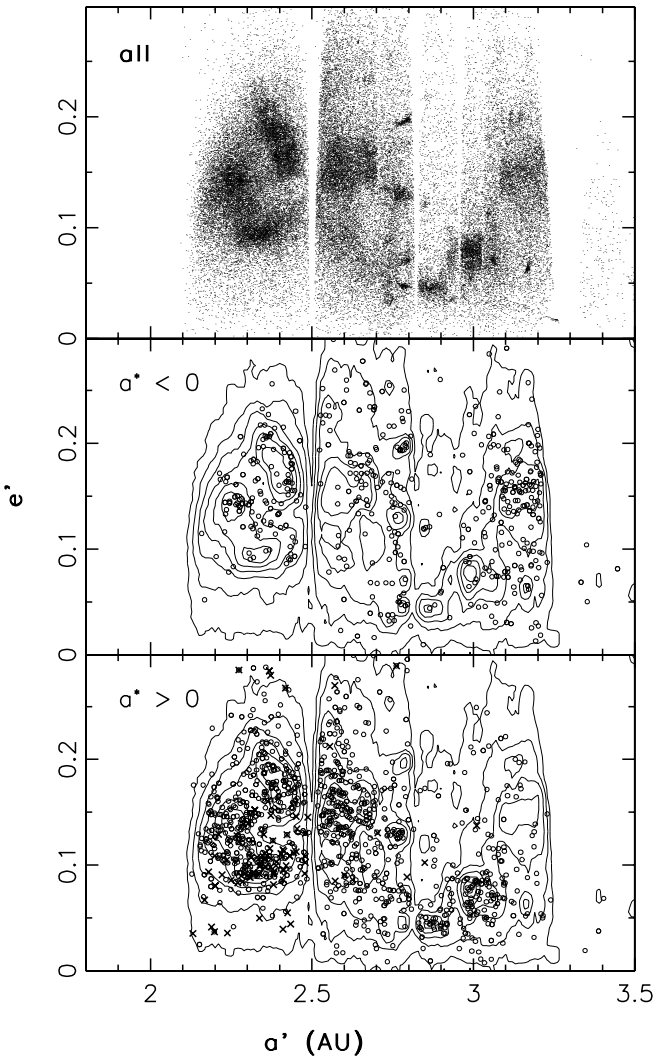

FIG. 11.—Same Fig. 10, but for the e' (eccentricity) vs. a' plane

The middle portion of the belt, between the 3 : 1 and 5 : 2 resonances ($2.5 < a' < 2.8$), contains a number of smaller families. The SDSS sample discussed here provides good color information for five of them. The Maria family is found to be red, with 16 out of 21 asteroids with $a^* > 0$. The more numerous Eunomia family also displays red characteristics (97 red and 7 blue members). On the other hand, the Adeona family and the Dora family are blue (12 out of 15, and all 11, members blue, respectively). The Ceres family seems to be a mix of both asteroid types, with 11 blue and 24 red asteroids. Other smaller families have fewer identified members; we find marginal evidence that the Hoffmeister, Rafita, and Hestia families are predominantly red, while the Misa and Taiyuan families are predominantly blue.

The inner part of the belt is dominated by the Vesta-Flora complex and at lower inclinations by the Nysa-Polana and Massalia families. The Nysa-Polana group is found to include a mix of red and blue asteroids, with red asteroids dominating the sample in an approximately 3 : 1 ratio (51 red and 19 blue). This is the strongest mixing of blue and red asteroids found for the families studied here and supports the claim by Cellino et al. (2001) that the Nysa-Polana group includes two independent families, one composed of S (red) asteroids and the other including low-albedo F-like (presumably blue) objects.

We note that for many families we find a substantial fraction ($\gtrsim 10\%$) of the minor component (e.g., $\sim$20% of the red Eos family members are blue). It is not easy to determine whether this mixing is due to background contamination (i.e., by asteroids that are not family members) or to nonhomogeneous structure of the parent bodies.[24] A robust analysis necessarily involves precise definitions of families and a careful study of the multidimensional color distribution for each family. Such an analysis is beyond the scope of this work and will be presented in a future publication.

[24] It is also possible that there is an asteroid color type that occupies the region around the boundary between blue and red types; see, e.g., Fig. 10 in I01.

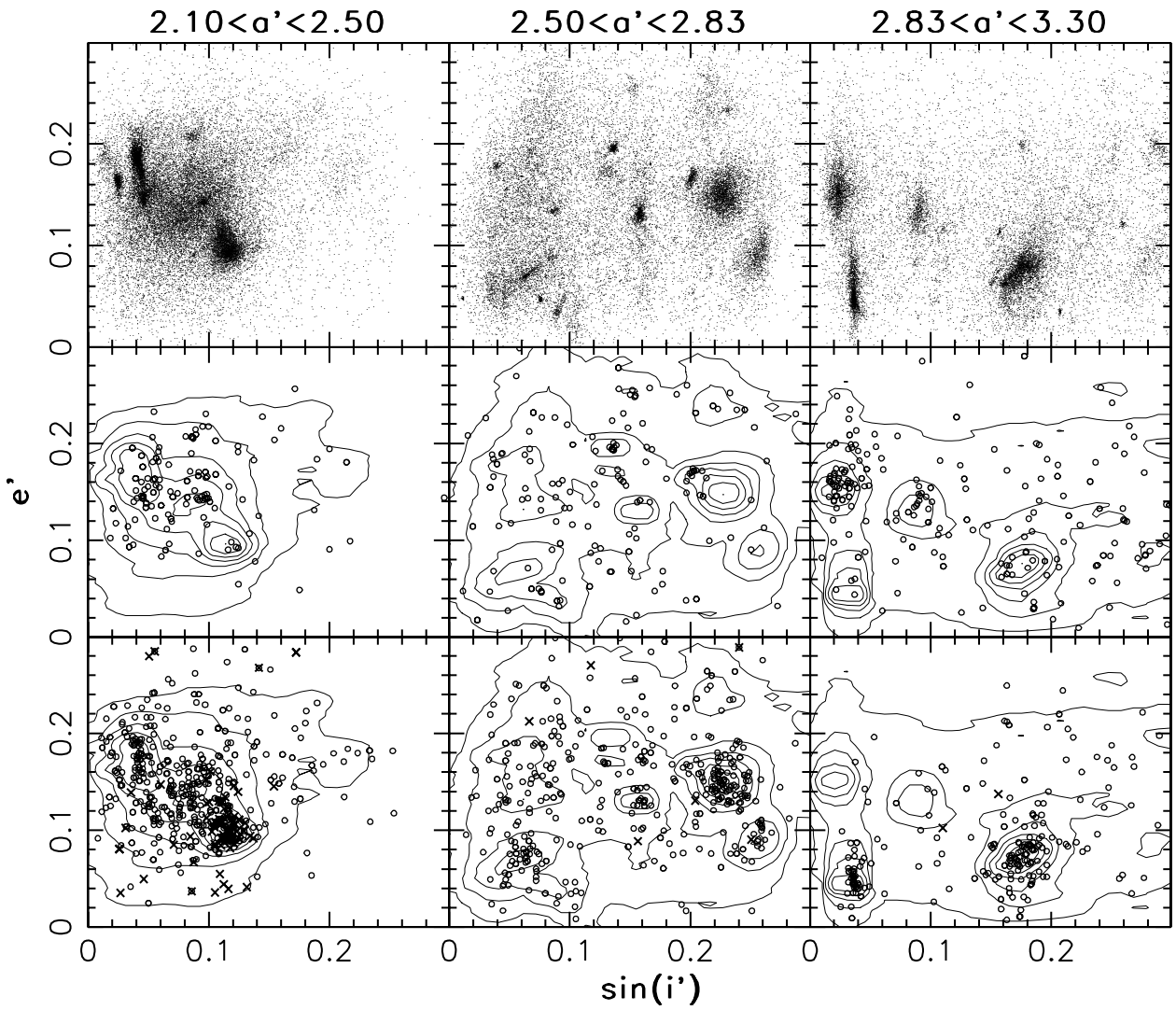

FIG. 12.—Same as Fig. 10, but for the e' vs. sin i' plane, and for three ranges of the semimajor axis, a', as marked at the top

4.3. *The V- and J-Type Asteroids*

I01 analyzed the distribution of 316 asteroids in SDSS color space by producing synthetic SDSS colors from the spectral measurements obtained by the SMASS project (Xu et al. 1995). In addition to the two major color types, there was an indication that red asteroids with extremely blue i^*-z^* colors may form a separate class (see Fig. 10 in I01). This notion was also supported by the taxonomic classification of asteroids with such colors; they were all classified as the J and V asteroids associated with the Vesta family (Binzel & Xu 1993). The proper orbital elements for 131 objects with $i^*-z^* < -0.25$ discussed here can be used to test whether these objects cluster in a'-sin(i')-e' space.

The Vesta family occupies a very small volume in the orbital parameter space centered at $a' \sim 2.35$, sin $i' \sim 0.12$, and $e' \sim 0.1$. If the asteroids with extreme i^*-z^* colors can be interpreted as J and V taxonomic types, then they should be concentrated in that region, rather than scattered throughout the belt as blue and red asteroids are. The 131 red asteroids with $i^*-z^* < -0.25$ are marked in Figures 10, 11, and 12 as crosses; it is evident that they are clustered around the Vesta family. This is better seen in Figure 13, where we show only the small region of the orbital parameter space that is relevant for the Vesta family ($2.1 < a' < 2.5$ and $0.09 < \sin i' < 0.15$). The red asteroids are shown as open circles, and the subset of 99 objects with $i^*-z^* < -0.25$ as crosses. The large filled circle marks the position of Vesta. The box outlined by the solid line is the core region ($2.28 < a' < 2.4$ and $0.1 < \sin i' < 0.13$), and the box outlined by the dashed line is the tail region ($2.4 < a' < 2.49$ and $0.1 < \sin i' < 0.13$) as proposed by Zappalà et al. (1995). Since a very high fraction of objects with $i^*-z^* < -0.25$ (99 out of 131 in the displayed region, and 50 and 29, respectively, in the outlined core and tail regions) are found in the region of the orbital parameter space that is associated with the Vesta family, we conclude that the i^*-z^* color provides a reasonably reliable method for selecting objects from the Vesta family.

5. DISCUSSION

This work demonstrates the feasibility of significantly increasing the number of asteroids with both accurate multicolor photometry and known orbital elements by matching SDSS-detected asteroids with the known asteroids. The sample discussed here includes ~2600 asteroids; when the SDSS is completed, the final catalog could be more than 10

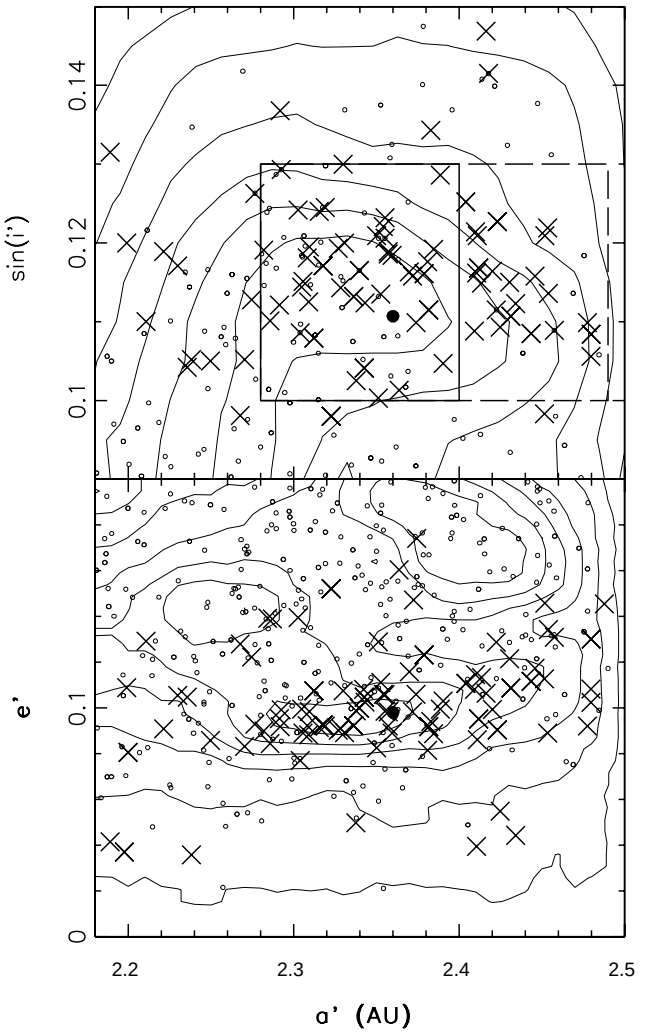

FIG. 13.—Regions from Figs. 10–12 that contain the Vesta family. Only objects with $a^* > 0$ are shown; those with $i^* - z^* < -0.25$ are marked by crosses, and others by circles. The boxes outline the core and the tail regions, as discussed by Zappalà et al. (1995). The position of Vesta is marked by a large filled circle.

times larger. Such a large sample can be used for a compositional analysis of the asteroid families at a level of detail that has not previously been possible. We show here that SDSS color information is sufficient to reveal strong color segregation among the asteroid families: most are dominated by either blue or red objects.

We showed that the SDSS photometric pipeline automatically flags ~90% of observed moving objects, with a contamination level of only a few percent. This is a better performance than for any other similar code. The directly determined completeness is lower than the 98% claimed in I01, though without any significant consequences for those results.

Only 66% of the known asteroids listed in the ASTORB file have sufficiently accurate orbital elements to predict their positions to better than 30″. However, most objects with unreliable orbital elements can be efficiently removed. It is much more perplexing that there is a large offset in magnitude scales, not only with respect to SDSS but also among the standard asteroid databases. This offset results in an overestimate of the number of asteroids brighter than a given magnitude limit by a factor of 1.7 and resolves the discrepancy between the SDSS asteroid count normalization and the number of asteroids listed in ASTORB.

We thank Robert Jedicke for fruitful discussions regarding the discrepancy in asteroid counts between SDSS and the ASTORB database, and Dejan Vinković for helping with the visual inspection of SDSS images. We are grateful to the referee, Ed Tedesco, for many insightful comments that helped improve the final version. We thank Princeton University for generous financial support of this research. Funding for the creation and distribution of the SDSS Archive has been provided by the Alfred P. Sloan Foundation, the Participating Institutions, the National Aeronautics and Space Administration, the National Science Foundation, the US Department of Energy, the Japanese Monbukagakusho, and the Max-Planck-Gesellschaft. The SDSS Web site is http://www.sdss.org/. The SDSS is managed by the Astrophysical Research Consortium for the Participating Institutions. The Participating Institutions are the University of Chicago, Fermilab, the Institute for Advanced Study, the Japan Participation Group, Johns Hopkins University, Los Alamos National Laboratory, the Max-Planck-Institut für Astronomie, the Max-Planck-Institut für Astrophysik, New Mexico State University, Princeton University, the US Naval Observatory, and the University of Washington.

REFERENCES

Binzel, R. P., & Xu, S. 1993, Science, 260, 186
Bowell, E., Hapke, B., Domingue, D., Lumme, K., Peltoniemi, J., & Harris, A. W. 1989, in Asteroids II, ed. R. P. Binzel, T. Gehrels, & M. S. Matthews (Tucson: Univ. Arizona Press), 524
Cellino, A., Zappalà, V., Doressoundiram, A., Di Martino, M., Bendjoya, P., Dotto, E., & Miglorini, F. 2001, Icarus, 152, 225
Chapman, C. R., Morrison, D., & Zellner, B. 1975, Icarus, 25, 104
Chapman, C. R., Paslicchi, P., Zappalà, V., Binzel, R. P., & Bell, J. F. 1989, in Asteroids II, ed. R. P. Binzel, T. Gehrels, & M. S. Matthews (Tucson: Univ. Arizona Press), 386
Fukugita, M., Ichikawa, T., Gunn, J. E., Doi, M., Shimasaku, K., & Schneider, D. P. 1996, AJ, 111, 1748
Hirayama, K. 1918, AJ, 31, 185
Ivezić, Ž., et al. 2001, AJ, 122, 2749 (I01)
Jedicke, R., Larsen, J., & Spahr, T. 2002, in Asteroids III, ed. W. Bottke, A. Cellino, P. Paolicchi, & R. Binzel (Tucson: Univ. Arizona Press), in press
Jurić, M., & Korlević, K. 2000, in Proc. 2d CARNet Users Conference, ed. M. Milinović, M. Matijašević, P. Pale, H. Stipetić, & M. Šmit (Zagreb: Organizira Hrvatska Akad. Istraživačka Mreža), No. G3
Krisciunas, K., Margon, B., & Szkody, P. 1998, PASP, 110, 1342
Lupton, R. H., et al. 2002, in preparation
Milani, A. 1999, Icarus, 137, 269
Milani, A., & Knežević, Z. 1992, Icarus, 98, 211
Muinonen, K., & Bowell, E. 1993, Icarus, 104, 255
Oke, J. B., & Gunn, J. E. 1983, ApJ, 266, 713
Pier, J. R., Munn, J. A., Hindsley, R. B., Hennessy, G. S., Kent, S. M., Lupton, R. H., & Ivezić, Ž. 2002, AJ, submitted
Standish, E. M. 1998, JPL Planetary and Lunar Ephemerides, DE405/LE405 (Interoffice Memo. 312.F-98-048) (Pasadena: JPL)
Stoughton, C., et al. 2002, AJ, 123, 485 (erratum 123, 3487)
Xu, S., Binzel, R. P., Burbine, T. H., & Bus, S. J. 1995, Icarus, 115, 1
York, D. G., et al. 2000, AJ, 120, 1579
Zappalà, V., Bendjoya, P., Cellino, A., Farinella, P., & Froeschlé, C. 1995, Icarus, 116, 291
Zellner, B. 1979, in Asteroids, ed. T. Gehrels (Tucson: Univ. Arizona Press), 783
Zellner, B., Tholen, D. J., & Tedesco, E. F. 1985, Icarus, 61, 355